Journal of Molecular Liquids 340 (2021) 117191

Contents lists available at ScienceDirect

Journal of Molecular Liquids

journal homepage: www.elsevier.com/locate/molliq

# Sunlight assisted photocatalytic degradation of different organic pollutants and simultaneous degradation of cationic and anionic dyes using titanium and zinc based nanocomposites

Radhakrishna S. Sutar, Rani P. Barkul, Meghshyam K. Patil *

*Department of Chemistry, Dr. Babasaheb Ambedkar Marathwada University, Aurangabad, Sub-campus Osmanabad-413 501, MS, India*

ARTICLE INFO

*Article history:*
Received 11 March 2021
Revised 9 July 2021
Accepted 3 August 2021
Available online 08 August 2021

*Keywords:*
Nanocomposite
Hydrothermal process
$Zn_2TiO_4$
ZnO-$TiO_2$
Photocatalyst
Dye degradation

ABSTRACT

ZnO-$TiO_2$ nanocomposites have been successfully synthesized by using simple hydrothermal method with various ZnO-$TiO_2$ concentrations (such as 2:1, 1:1 and 1:2 ZnO-$TiO_2$, pure ZnO and $TiO_2$). The XRD, FT-IR, HR-TEM, FE-SEM with EDAX, XPS and UV–Visible spectroscopy were utilized for characterization of the as-prepared products. XRD revealed that samples are in nanocrystalline nature with formation of anatase $TiO_2$, hexagonal ZnO, cubic $Zn_2TiO_4$ and other zinc titanates. The average crystallite size of the samples was between 8 and 36 nm. The photocatalytic activity has been demonstrated for the degradation of methylene blue (MB), tetracycline (TC) and mixture of dyes (includes methylene blue, rhodamine B and methyl orange) under sun light irradiation at room temperature. The degradation rate of methylene blue has been significantly enhanced with increase in percentage of ZnO. Nanocomposites with 2:1 concentration of Zn and Ti, has been more efficient than that of other composites. Also, effect of different parameters such as pH of dye solution, concentration of dye and amount of catalyst etc. has been evaluated.



## 1. Introduction

Currently whole world suffering from environment issue such as lack of substantial and clean natural energy, pollution, contamination of the environment. The fast growing industrializations have increased the generation of highly toxic and carcinogenic wastewater. The wastewater includes high concentration of various organic dyes, surfactants, heavy metals and other harmful compounds which also hazardous to the quality of soil and introduce ill-effect on aquatic ecosystems as well as human beings [1]. From them dyes and pigments are substances with high application potential in the various industries and extensively used in textile, food, cosmetic, precious stones, leather, paper, plastics, processing, printing, rubber, pharmaceutical, tannery primarily to color the final products [2]. During the process of colouring, 10–50% dyes are losses and discharged in to the wastewater that generate coloured effluents. For example, it is estimated that there are more than 100,000 synthetic dyes, with an annual manufacture of more than 700,000 tons world-wide, producing a significant amount of wastewater [3]. In the textile effluent the concentration of dyes are differs from 10 mg/L to 250 mg/, the highest concentration 800 mg/L of reactive dye referred by Yaseen and Scholz [4,5]. Furthermore, tetracycline (TC) is frequently used as antibiotics, which on discharge to water system develops considerable adverse effects on human health and ecological systems. Due to the poor decomposition in animals and human bodies, the majority of TC is discharged into the wastewater [6]. Furthermore, antibiotic existence in the environment can affect various species of bacteria, and increase their resistance [7], thus it needs appropriate approaches for its removal.

Numerous technologies have been widely investigated to remove the concentration of dye and tetracycline from wastewater. In which photocatalytic technology is an emerging and severally demonstrated with prominent superiority for the decomposition of organic dyes, pollutants and pharmaceutically emerging contaminants from different industries, health care sector as well as agriculture field. Semiconductor composite photocatalysts have been extensively exploited in recent years owing to their promising properties due to individual components and newly introduced properties due to formation of composite. Several composites has been used for addressing the pressing task to curb the current rapid deterioration of the living environment [8]. Primarily, in photocatalysis decomposition of organic and inorganic compounds has been initiated through the generation of electron-hole pairs. Photocatalyst illuminated with light of energy

* Corresponding author.
*E-mail address:* meghshyam_patil@yahoo.com (M.K. Patil).

https://doi.org/10.1016/j.molliq.2021.117191
0167-7322/

higher than its band gap, which results in excitation of electrons from the valence band (VB) to the conduction band (CB), leaving holes in the VB. These photo excited electrons and the generated holes could help to deoxidize or oxidize adsorbates on the catalyst surface.

Among various semiconductor photocatalysts, titanium oxide ($TiO_2$), especially with the anatase phase, is one of the most attractive and exploited catalyst due to its several properties, which includes chemical stability, inexpensiveness, high crystallinity, strong oxidation and reduction properties, non-toxicity, and light-scattering properties [9,10]. However, $TiO_2$ has a wide band gap energy (3–3.2 eV). It limits the photocatalytic applications of $TiO_2$ under sunlight irradiation as it needs ultraviolet light for activation and generally sunlight having less than 5% UV light [11]. From last few decades, improving $TiO_2$ photocatalytic efficiency has become a hot topic. One of commonly used approach is doping of transition metals/non-metals into $TiO_2$, forming doped photocatalyst, which would modify both physical and optical properties of $TiO_2$ [10,12,13]. Another approach is to couple the $TiO_2$ with other oxides in order to achieve higher photocatalytic efficiency. These metal oxides includes $WO_3$ [14], $ZrO_2$ [15], ZnO [16–18], $SiO_2$ [19,20], $Fe_2O_3$ [21], $SnO_2$ [22] and $MoO_3$ [23]. Like $TiO_2$, zinc oxide (ZnO) is another promising n-type semiconductor photocatyst, which has received a great attention. ZnO having wide band gap of 3.37 eV and used efficiently for organic pollutants photodegradation[24–31]. Further, it is attracting researcher due to its nontoxicity, high catalytic efficiency and low cost [32–35]. But, due to large band gap energy ZnO photocatalyst is also applicable under UV irradiation [36]. Also, ZnO suffers from intrinsic drawback of photocorrosion, which resembles its photoactivity and photostability [37]. Further, several research activities have been applied to enhance the photocatalytic properties by introducing nanostructures or morphologies of $TiO_2$ as well as ZnO [38–40], including polymer backing [41], surface doping with nonmetallic/metallic elements or semiconductor oxides [10,12,13,42–45], and surface deposition/composites of metal nanoparticles [46–48]. $TiO_2$ catalyst can be coupled with ZnO in the form of composite to enhance photocatalytic efficiency by reducing the charge carrier recombination rate and improving its visible-light photocatalytic activity [49–51].

Furthermore, coupling of nanosized $TiO_2$ and ZnO has been well-established and remarkably improve the separation efficiency of photo excited charge carriers due to the formation of heterojunction structure between these two, thus improving quantum efficiency as well as photostability of the catalyst [52,53]. Though the binding energies of ZnO and $TiO_2$ are comparable to each other, the potentials of the CB and the VB of ZnO are bit more negative than those of $TiO_2$ [54,55]. Accordingly, lower band gap energy may be achieved when $TiO_2$ and ZnO were combined in an appropriate way [56,57].

ZnO-$TiO_2$ nanostructured composites were very active materials due to its unique properties. These nanocomposites were multifunctional semiconductor materials with a direct wide-band gap and large excitation binding energy. Nanostructured semiconductor ZnO-$TiO_2$ nanocomposite were synthesized using various techniques like sol–gel, hydrothermal, solution combustion, co-precipitation, ultrasonic precipitation, ball milling technique, and thermal decomposition [58–62].

In this present study, we have developed a facile and reproducible strategy for preparing ZnO-$TiO_2$ and ZnO/$Zn_2TiO_4$ nanocomposites by hydrothermal method. The prepared nanocomposites were characterized by X-ray diffraction spectroscopy (XRD), Fourier transform infrared spectroscopy (FTIR), Scanning electron microscopy (SEM), Energy-dispersive X-ray spectroscopy (EDX), high resolution transmission electron microscopy (HRTEM), and UV–Vis diffuse reflectance spectroscopy (UV-DRS), etc. The photocatalytic activity of the as-prepared photocatalyst was measured by the degradation of methylene blue (MB), mixture of dyes and tetracycline antibiotic. The nanocomposites displayed significantly enhanced photocatalytic activity than pure $TiO_2$ under direct sun light irradiation.

## 2. Experimental procedure

### 2.1. Synthesis of Catalysts:

#### 2.1.1. Preparation of mixture A:

5.60 g of zinc acetate dihydrate was dissolved in 50 ml water under vigorous stirring at 60 °C. 10 ml 0.5 M sodium hydroxide solution was added dropwise into zinc acetate aqueous solution until a transparent solution was obtained (at pH = 9). Resultant solution was stirred at 60 °C for 30 min.

#### 2.1.2. Preparation of mixture B:

The 7.593 ml of acetic acid was added in to 75 ml of ethanol under continuous stirring for 30 min. Then 7.593 ml of titanium tetra-isopropoxide was also added to acetic acid solution and stirred for 30 min. at room temperature.

The prepared mixture B solution was dropwise added to mixture A under constant stirring at 60 °C for 30 min. This mixture was then transferred into a stainless steel autoclave and maintained at 150 °C for 18 h. After cooling to room temperature, the formed white precipitate was filtered, washed with distilled water and ethanol and dried in the oven at 80 °C. Finally, obtained powder was calcined at 450 °C for 6 h.

By this developed procedure, we prepared nano-composites by taking 1:1, 1:2 and 2:1 M ratio of Ti and Zn and designated as ZnTi-1:1, ZnTi-2:1 and ZnTi-1:2 respectively.

### 2.2. Characterization

The phase compositions and crystallinity of the products were investigated by powder X-ray diffraction (XRD) measurement on a X-Ray diffraction system Ultima of Rigaku Corporation. Line traces were collected over 2θ values ranging from 20° to 80°. The vibrational modes were determined by FTIR spectra of the nanocomposites by using FT-IR spectrometer thermo electron scientific (Nicolet iS10 Mid) in the range of 400–4000 $cm^{-1}$. Morphologies of the products were examined by a field-emission scanning electron microscope (FEI Nova nano SEM 450) and a high-resolution transmission electron microscope 300 kV equipped (Rigaku Corporation). The chemical composition of the products was also investigated using energy dispersive X-ray analysis (EDS) (Bruker X-flash 6130). The UV–Vis spectra of the catalysts and photocatalytic degradation studies of the dyes and mi under study were performed on a Elico UV–visible spectrophotometer (UV–Vis; Elico, model v670). XPS measurement of the prepared sample have been recorded on a Shimadzu (ESCA 3400) spectrometer having Mg Ka (1253.6 eV) radiation as the excitation source.

### 2.3. Photocatalytic degradation

The photocatalytic activity of the ZnTi-1:1, ZnTi-2:1, ZnTi-1:2 nano-composites and bare $TiO_2$ has been tested for the degradation of MB and mixed dyes (20.0 mg/L) in aqueous solution under sunlight irradiations. Also various parameters of reaction mixture such as concentration of dye, amount of catalyst, pH of dye solution, etc. were optimized during photo degradation reaction. The pH of the MB dye solution was varied by adding required amount of 1 N NaOH or 1 N HCl solution.

*2.3.1. Photocatalytic degradation of MB*

The 200 ml (20 mg/L)MB solution was taken in 500 ml beaker containing 100 mg catalyst. Initially, this solution was stirred in dark for 30 min to achieve the adsorption desorption equilibrium and then kept in sun light. Sample was collected after given time intervals, also the colour of dye solution decreased with time. Absorbance of obtained samples were measured at wavelength 200–800 nm. For testing the self-photodegradation of dye solution, 200 ml dye solution was kept in sun light for about 7 h. Observation indicates that reaction does not proceed without catalyst.

*2.3.2. Photocatalytic degradation of mixed dyes*

Photodegradation reaction was carried out with mixed dyes (a solution of methyl orange, methylene blue, rhodamine B). Mixture of dye solution has been prepared by taking equal volume of each dye solution and 20 ppm stock solution of individual dye have been used. 200 ml (20 mg/L) of mixed dye solution was taken in round bottom flask. Initially, for testing self-degradation of these dyes, the assembly was kept in sunlight without catalyst, no change in colour and absorbance was observed after 7 h. Then, 100 mg catalyst was added into the reaction and assembly was kept in dark at room temperature for 30 min and then whole assembly was kept in sunlight. The samples were collected at definite time intervals and centrifuged and monitored by using UV–visible spectrophotometer at wavelength 200–800 nm.

*2.3.3. Photocatalytic degradation of tetracycline*

Furthermore, photocatalytic activity of the prepared nanocomposite ZnTi-1:2 was also tested for the degradation of tetracycline antibiotic under sunlight irradiation. The 20 ppm solution of tetracycline was prepared and control experiments were carried out with using 200 ml solution with stirring without using catalyst in sunlight for a day. By maintaining same condition, the reaction did not proceed and the concentration of tetracycline solution remained intact. Then the reaction solution was prepared by using 100 mg ZnTi-1:2 nanocomposite and 200 ml solution of 20 ppm tetracycline antibiotic. Firstly, assembly was kept in dark with stirring at room temperature for 30 min to reach the adsorption–desorption equilibrium, then the reaction assembly was kept in sunlight. Samples were taken at definite time intervals and centrifuged and monitored by UV–Visible spectrometer for wavelength range 200 to 800 nm.

## 3. Results and discussion

*3.1. Characterization*

*3.1.1. X-ray diffraction study:*

The X-ray diffraction patterns of ZnO, $TiO_2$ and ZnTi-1:1, ZnTi-2:1, ZnTi-2:1 are shown in Fig. 1. Bare ZnO has shown the characteristic peaks at 31.81°, 34.5°, 36.32°, 47.65°, 56.69°, 62.93°, 68.00° and 69.23°, which are correspond to (100), (002), (101), (102), (110), (103), (112) and (201) crystal planes respectively, associated with wurtzite type of ZnO, which indicate that ZnO possesses a hexagonal crystal structure. Whereas, for pure $TiO_2$ diffraction peaks are located at 2θ = 25.25°, 36.89°, 37.79°, 47.99°, 53.94°, 55.09°, 62.70°, 68.77°, 70.26° and 75.14° which are corresponding to the following crystal planes (101), (103), (004), (200), (105), (211), (204), (216), (220) and (224), respectively and confirm the presence of anatase $TiO_2$. XRD analysis of ZnTi-1:2 indicate the presence of hexagonal ZnO and anatase $TiO_2$, confirming the formation of ZnO/$TiO_2$ composite. The results are compared with JCPDS (21–1272) and JCPDS (36–1451) for $TiO_2$ and ZnO respectively [63]. Also, XRD spectra of ZnTi-1:1 and ZnTi-2:1 has shown the presence of hexagonal ZnO. Interestingly, these two samples

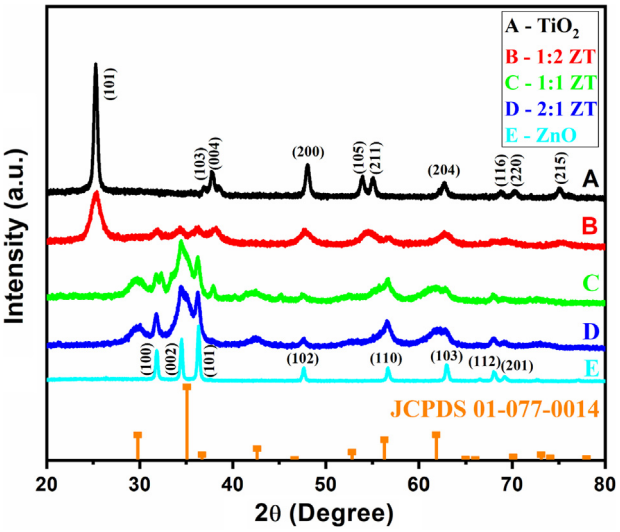


**Fig. 1.** XRD spectra of bare $TiO_2$, ZT-2:1,ZT-1:1, ZT-1:2 and bare ZnO powders.

additionally shown reflection peaks at 30.05° (220) and 42.48° (400) attributing to formation $Zn_2TiO_4$ phase, having a cubic phase (JCPDS 01–077-0014). Also, sample ZnTi-1:1 has shown additional peaks, which shows the presence of different zinc titanates such as $ZnTiO_3$, $Zn_2Ti_3O_8$. All these phases have been confirmed from literature [64–67]. From XRD, sample ZnTi-1:2 is ZnO/$TiO_2$ nanocomposite, while ZnTi-2:1 is $Zn_2TiO_4$/ZnO nanocomposite.

The crystallite size of the samples was calculated by using the Scherrer formula by considering highest intensity peak in each spectra:

$$D = k\lambda/\beta\cos\theta \quad (1)$$

Where D is crystallite particle size, k is a constant of 0.94, λ is the wavelength (nm) of X-rays, β is the full width at half-maximum of (101) peak, and θ is the Bragg angle [68]. The average crystallite size of the ZnTi-2:1, ZnTi-1:1, ZnTi-1:2, pure $TiO_2$ and pure ZnO was 8.32, 10.77, 11.47, 20.28 and 35.85 nm respectively.

*3.1.2. UV–Visible Study:*

Fig. 2 illustrates the UV–Visible spectra of bare $TiO_2$ and different prepared nanocomposites with different concentrations of Ti and Zn. From the figure, it has been clear that the prepared heterojunction nanocomposites has higher absorption than bare $TiO_2$. All the absorbance spectra has shown a sharp band at near to the 400 nm as absorption edge and slight red shift has been seen for composites as compare to bare $TiO_2$. As a result, these nanocomposites has shown slight variation of band gap energy as compared to that of bare $TiO_2$ (Fig. 2 (b)). The band gap of the prepared composites has been deduced by using the Tauc plot. The band gap energy has been obtained by plotting $(\alpha h\nu)^2$ vs. hν (where α is the absorption coefficient and hν is photon energy) and by extrapolation of the linear portion at $(\alpha h\nu)^2 = 0$ as shown in Fig. 2 b). The estimated band gap energy from the intercept of the tangents to the plots are 3.39, 3.29, 3.20 and 3.16 eV for the samples bare $TiO_2$, ZT-1:2, ZT-1:1 and ZT-2:1 respectively. As a result, the minimum energy is required to excite an electron from VB to CB is noticeably lower in the ZT-2:1 than that of the other composites and bare $TiO_2$. This concludes that the ZT-2:1 has a larger redox potential for the photocatalytic degradation of organic contaminants under sun light irradiation. Pictorial representation of conduction band and valence band for ZnO/$TiO_2$ and $Zn_2TiO_4$/ZnO nanocomposites has been shown in Fig. 3. As per XRD study these two schematics are represented by catalysts ZnTi-1:2 and ZnTi-2:1 respectively.

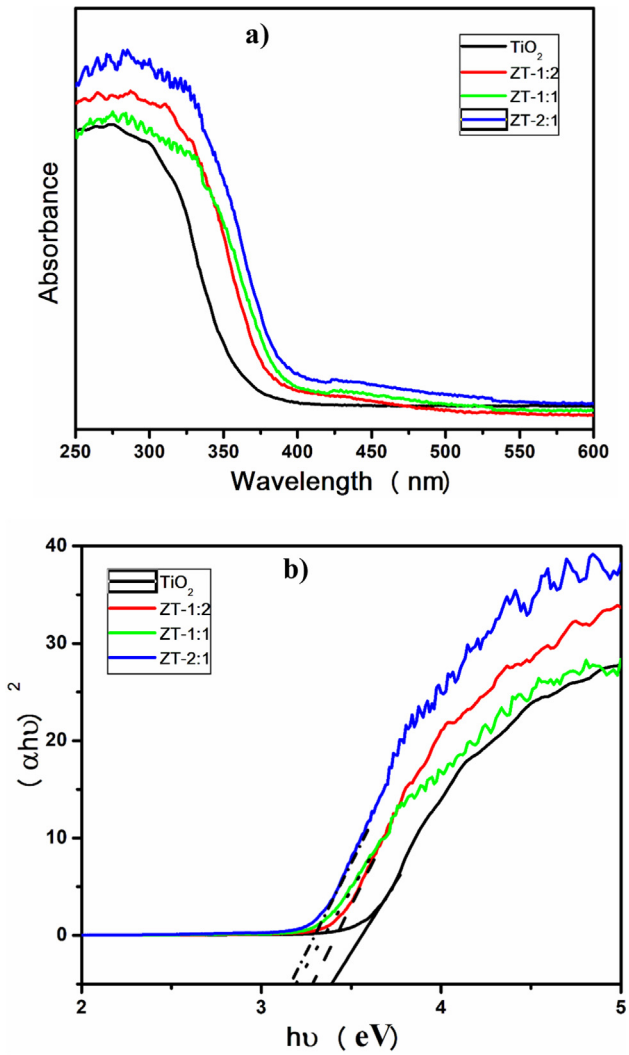


**Fig. 2.** Band gap energy measurement: a) UV–Visible absorption spectra and b) plot of $h\upsilon$ vs $(\alpha h\upsilon)^2$ of as-prepared catalysts.

*3.1.3. FT-IR studies:*

Fig. 4 shows the FT-IR spectrum of the ZT-1:2, ZT-1:1 and ZT-2:1 nanocomposites. The FT-IR patterns for all the samples are approximately parallel. The characteristic vibrations at ~ 500 and ~ 520 $cm^{-1}$ attributing to M–O stretching ie. Zn–O and Ti–O of nanocomposites, which are consistent with the results from previous reports [69]. Further, the FT-IR spectra of nano-composites, ZT-2:1, ZT-1:1 and ZT-1:2, exhibited weak bands at about 1377, 1447 and 1512 $cm^{-1}$ due to the presence of small amount of the organic residue during preparation methodology. Additionally, bands at about 1630 to 1730 $cm^{-1}$ and broadband centered at ~ 3380 $cm^{-1}$ corresponding to bending and stretching frequencies of the OH– groups on the surface of the prepared catalysts.

*3.1.3.1. Field Emission Scanning Electron Microscopy (FESEM) and EDAX measurements:.* Scanning electron microscopy has been used to study the morphology, shape and size of the prepared materials. Fig. 5 shows the FESEM images and EDAX spectra of the prepared photocatalysts ZT-1:2, ZT-1:1 and ZT-2:1. Fig. 5 (a and b) represents the images of photocatalysts ZT-1:1 and ZT-2:1, which shows the formation of nano-rod along with the highly agglomerated nanoparticles. Furthermore, Fig. 5 (c) representing the photocatalyst ZT-1:2, having spherical nanoparticles, which are also highly agglomerated. As the composition of catalyst is very sensitive for the application; the elements present in the nanomaterials were analyzed by energy dispersive X-ray spectroscopy (EDS). The EDS spectra of the as-prepared materials were recorded in the binding region of 0–12 keV. EDS analysis confirms the presence of Ti, Zn and O elements in formed composites. Elemental percentage obtained from the EDAX are shown in the table 1, which are comparable to preparation conditions.

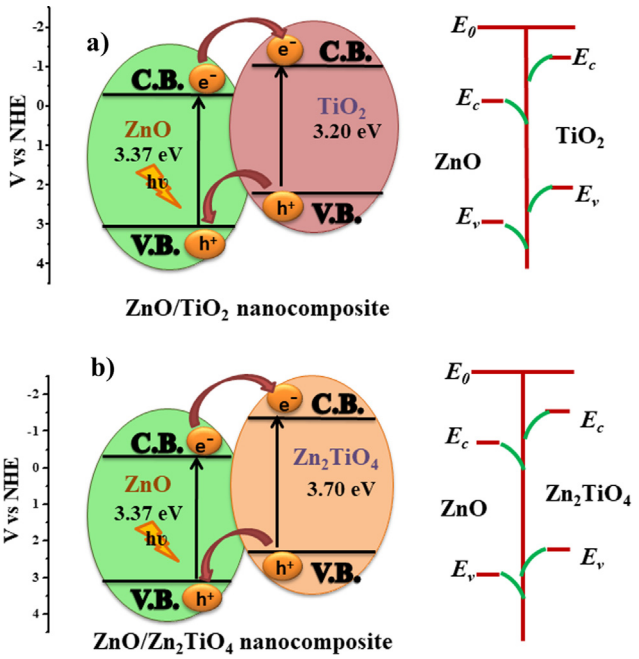


**Fig. 3.** Representation of VB and CB in $ZnO/TiO_2$ and $ZnO/Zn_2TiO_4$ nanocomposites ($E_0$, $E_c$ and $E_v$ represents energy levels of CB top, CB low and VB top respectively).

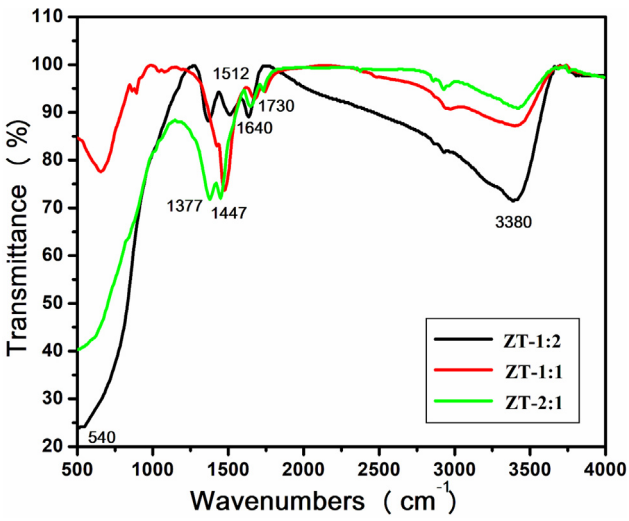


**Fig. 4.** FT-IR spectra of the ZnO-$TiO_2$ (2:1, 1:1 and 1:2) nanocomposites.

*3.1.4. High-resolution transmission electron microscopy (HRTEM):*

HRTEM images at different resolution for ZT-2:1 has been shown in Fig. 6. HRTEM images has shown the nano-crystalline particles aggolamerization. Particle size distribution plot from Fig. 6 b) is shown in Fig. 6 c) and indicate that the average particle size in from 8 to 11 nm which is also in accordance with the results obtained from XRD.

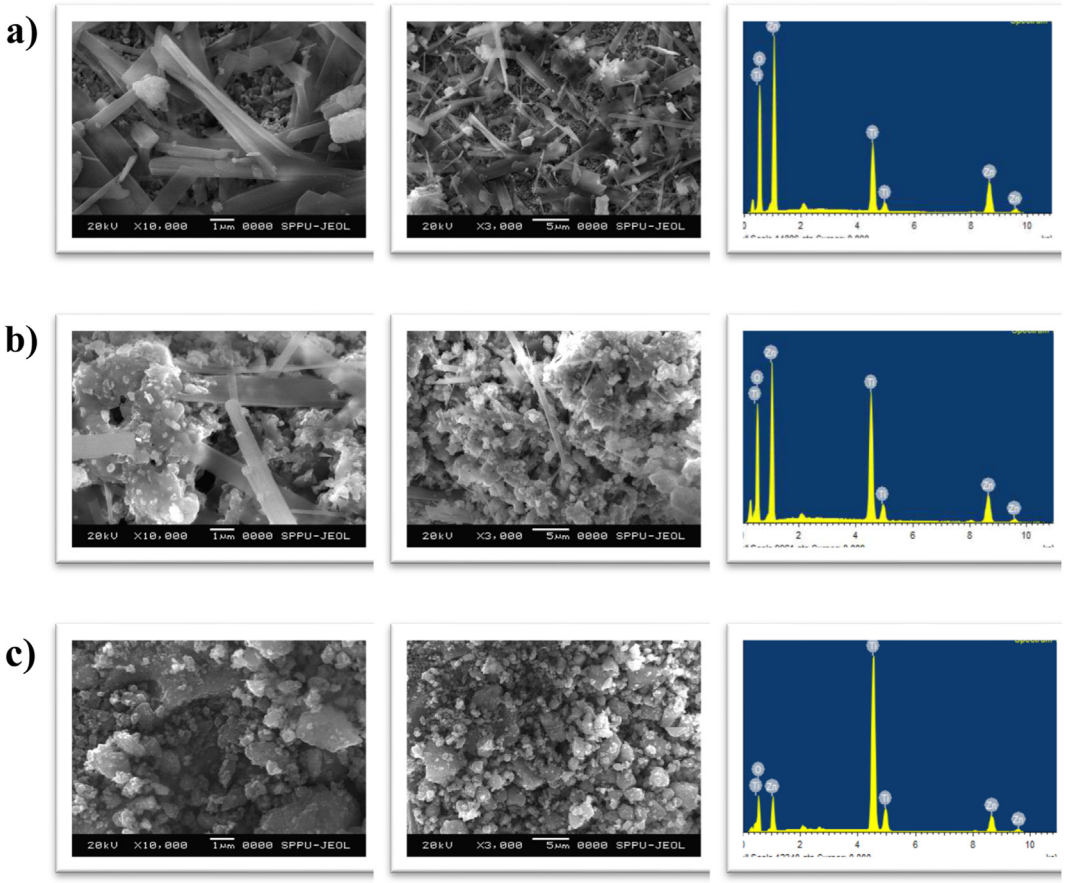


**Fig. 5.** FESEM images and EDAX spectrum of the a) ZT-2:1, b) ZT-1:1 and c) ZT-1:2 nanocomposites.

**Table 1**
Elemental composition analysis of ZnTi-2:1, ZnTi-1:1, ZnTi-1:2 nanocomposites.

| Nanocomposite | Elemental composition (atomic %) | | |
|---|---|---|---|
| | Zn-element | Ti-element | O-element |
| ZnTi-2:1 | 9.88 | 5.14 | 84.98 |
| ZnTi-1:1 | 5.70 | 8.12 | 86.18 |
| ZnTi-1:2 | 5.66 | 18.63 | 75.71 |

*3.1.5. X-ray photoelectron spectroscopy:*

Fig. 7 shows the XPS analysis of ZT-2:1 sample, which confirms the elemental composition of as-prepared catalyst. Fig. 7 a) shows the survey spectra, which indicates the presence of Ti, Zn and O in the sample. In Fig. 7 b), the peaks at 458.4 eV and 464.2 eV represents $Ti^{4+}$, which are corresponds to Ti $2p_{3/2}$ and Ti $2p_{1/2}$ respectively. As shown in Fig. 7 c), the first peak at 530.1 eV is corresponding to lattice oxygen associated with $Ti^{4+}$ and $Zn^{2+}$. The second peak at 531.6 eV is attributed to oxygen from the surface hydroxyl group in the catalyst and last peak at 535.7 eV assigned to the moisture absorbed in the samples. In Fig. 7 d), the binding energy peaks at about 1021.5 eV and 1044.7 eV are corresponds to the valance state of $Zn^{2+}$, which are attributed to Zn $2p_{3/2}$ and Zn $2p_{1/2}$ respectively. Similar results have been found in the literature [70].

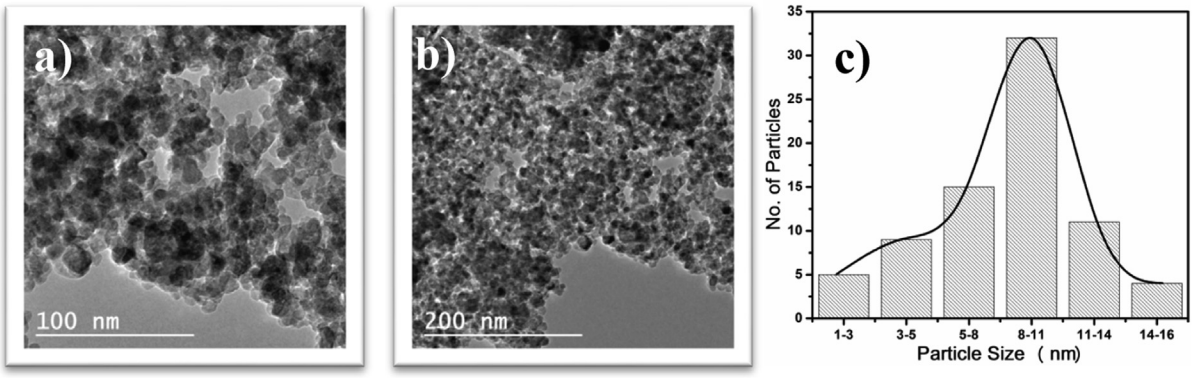


**Fig. 6.** HRTEM images of ZT-2:1 nanocomposite and corresponding particle size distribution.

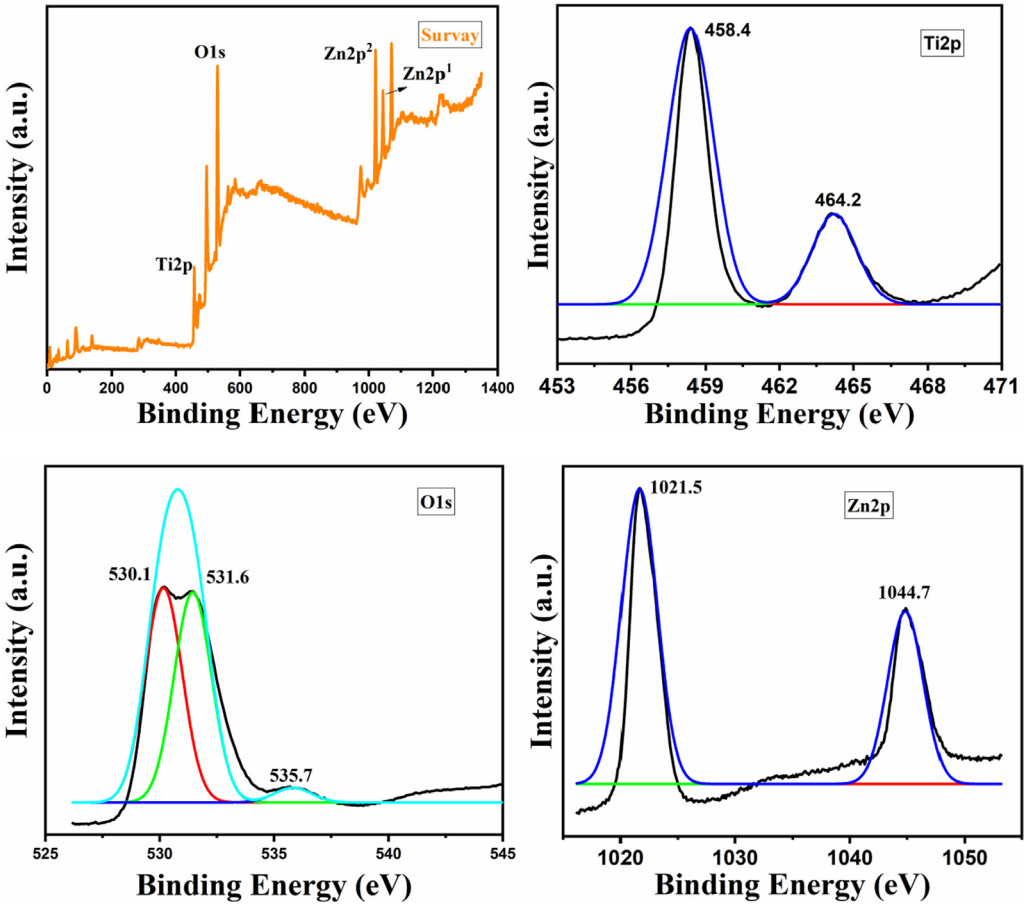


**Fig. 7.** a) XPS spectra of ZT-2:1 nanocomposite, high-resolution spectra of b) Ti 2p, c) O 1 s, d) Zn 2p.

### 3.2. Photocatalytic degradation of MB dye:

Photocatalytic degradation of MB dye has been studied by using photocatalysts ZT-1:2, ZT-1:1, ZT-2:1 and bare $TiO_2$. MB is one of the important dye used in textile industries and contributing for water pollution. We have used MB as a representative of industrial dye for photocatalytic study. Initially, in blank experiment, we have carry out the experiment in sunlight without any photocatalyst and no degradation of MB has been observed. Further, we have studied the degradation of 20 ppm MB solution using prepared photocatlysts. Fig. 8 shows the degradation trend of MB dye using ZnTi-2:1 photocatalyst, examined by using UV–visble spectroscopy and complete degradation has been observed in 150 min. Fig. 9 a), shows the degradation results obtained by using various catalysts. ZnTi-2:1 catalyst has shown the higher degradation efficiency as compare to other catalysts. The higher efficiency of ZnTi-2:1 is may be due to less particle size and lower band gap of the catalyst. Further, Fig. 9 b) shows that the degradation of MB dye using these catalysts is pseudo first order reaction and appearent rate constant has been calculated by equation:

$$-\log\frac{C_0}{C} = K_{app.}\frac{t}{2.303}\cdots \quad (2)$$

Where, $K_{app}$ is the apparent rate constant of a reaction, $C_0$ is the initial concentration of MB dye solution and C is the concentration of MB dye solution at reaction time t.

Obtained rate constants of the degradation experiments has been shown in table 2. From the kinetic study, rate constant for degradation by using ZnTi-2:1 is 28.92 $\times$ $10^{-3}$ $min^{-1}$, which is almost double than that of ZnTi-1:2 catalyst (14.28 $\times$ $10^{-3}$ $min^{-1}$) and also higher than all the prepared catalysts. By using ZnTi-2:1 catalyst, we have studied the effect of various reaction parameters such as concentration of dye, pH of dye solution, and catalyst loading.

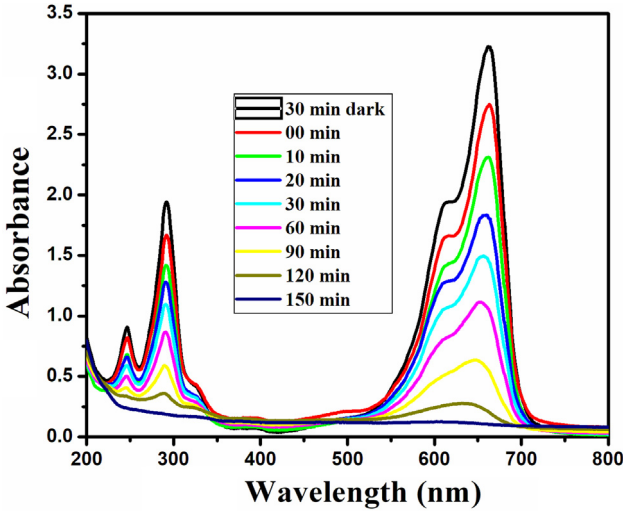


**Fig. 8.** UV–Visible spectra of MB using ZT-2:1 catalyst at different time interval.

Degradation study has been performed by using 20, 30 and 40 ppm solution of MB dye and the obtained results are shown in Fig. 10. On increasing the concentration of dye, more number of dye molecules are available for degradation, which will show

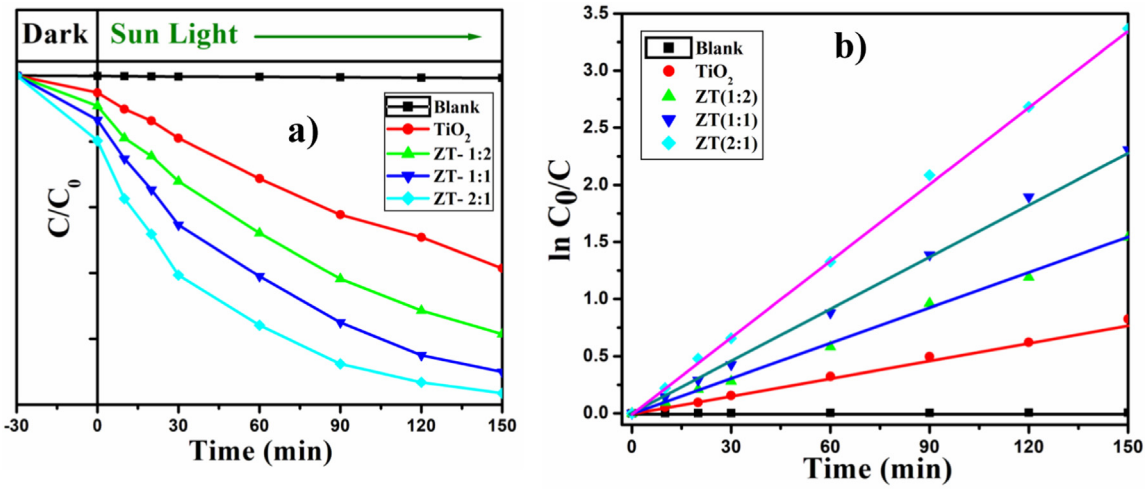


**Fig. 9.** a) Plot of $C/C_0$ *vs* time (min.) for all catalysts and b) corresponding plot of $\ln C_0/C$ *vs* time (min.).

**Table 2**
Reaction kinetic parameters for degradation of MB dye using as-prepared catalysts.

| Catalyst | Initial dye concentration (%) | Remaining dye concentration after 150 min. (%) | Rate constant ($min^{-1}$) |
|---|---|---|---|
| $TiO_2$ | 100.0 | 43.74 | $5.27 \times 10^{-3}$ |
| ZT-1:1 | 100.0 | 11.51 | $14.28 \times 10^{-3}$ |
| ZT-1:2 | 100.0 | 23.63 | $9.74 \times 10^{-3}$ |
| ZT-2:1 | 100.0 | 4.31 | $28.92 \times 10^{-3}$ |

positive effect on degradation efficiency, whereas due to colour intensity, it may restrict the incoming light to reach the catalyst, which results in decrease in degradation efficiency. Both these factors works during the study of degradation of dye at different concentration. From Fig. 10 a) degradation of 20 ppm solution comparatively takes place faster as compare to 30 ppm and 40 ppm solution, but from Fig. 10 b) it has been clear that rate of degradation ie. d[MB]/dt is increasing with increase in concentration. Furthermore, as time goes on for each experiment rate of degradation decreases.

To study the role of pH on degradation efficiency, we have adjusted the pH of the solution by adding 0.1 N HCl and 0.1 NaOH. Experiments has been carried out at pH 1, 5, 9 and 11. From the Fig. 11, it has been clear that in basic pH degradation efficiency is more as compare to acidic pH. Also, this observation support that, $^{\bullet}OH$ formed due to addition of NaOH, may play an important role in degradation mechanism. Further, basic and acidic condition can deprotonate and protonate the surface of catalyst respectively. As a result, the surface become negatively and positively charged in alkaline and acidic medium respectively. The generated charge on the surface can change the adsorption of organic pollutant on the catalyst surface, which can change the rate of reaction. As degradation is faster in basic pH, the reactive species $OH^{\bullet}$, generated on the surface of the catalyst is responsible for the degradation of the organic pollutants under sunlight. The formation $OH^{\bullet}$, $HO_2^{\bullet}$ and $O_2^{-\bullet}$ radicals takes place on the surface of the catalyst under different conditions as shown in equations (3–6). The degradation of organic pollutant takes place photo catalytically as shown in equations due to formation of $OH^{\bullet}$ as shown in equations (7–9).

$$e^{-}_{CB} + O_2(aq) \rightarrow O_2^{-\bullet} \quad (3)$$

$$e^{-}_{CB} + O_2(aq) + H^{+} \rightarrow HO_2^{\bullet} \quad (4)$$

$$h^{+}_{VB} + OH^{-} \rightarrow OH^{\bullet} \quad (5)$$

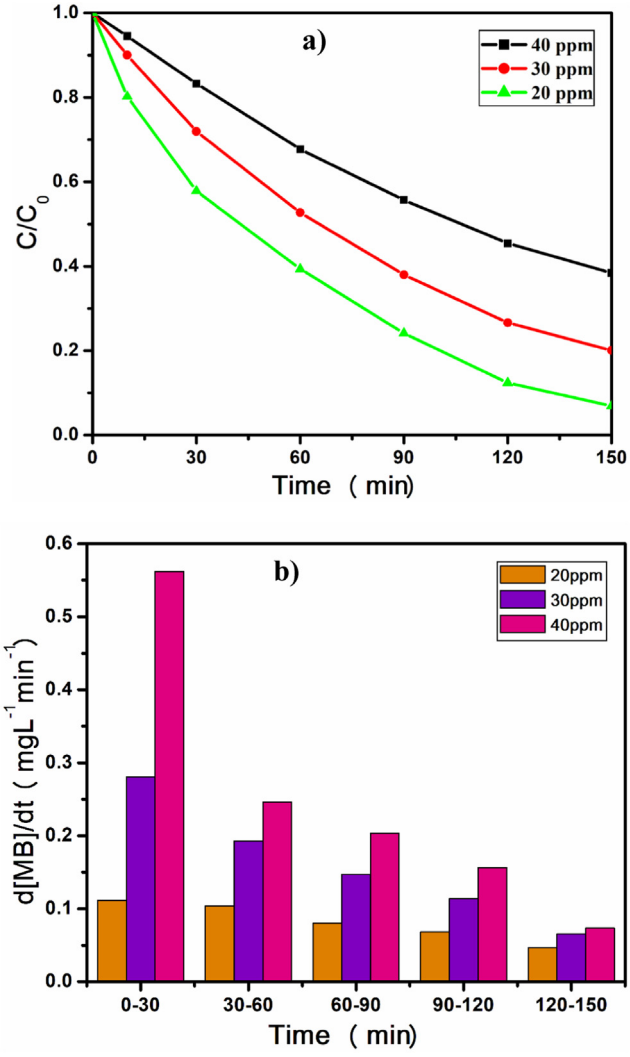


**Fig. 10.** Degradation of MB dye using different concentration and ZT-2:1 as catalyst: a) plot of $C/C_0$ *vs* time b) plot of d[MB]/dt *vs* time.

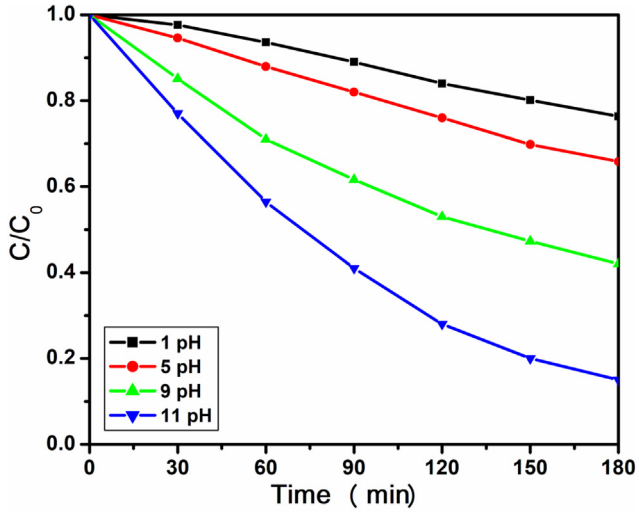


**Fig. 11.** Degradation of MB dye at different pH of solution and ZT-2:1 as catalyst.

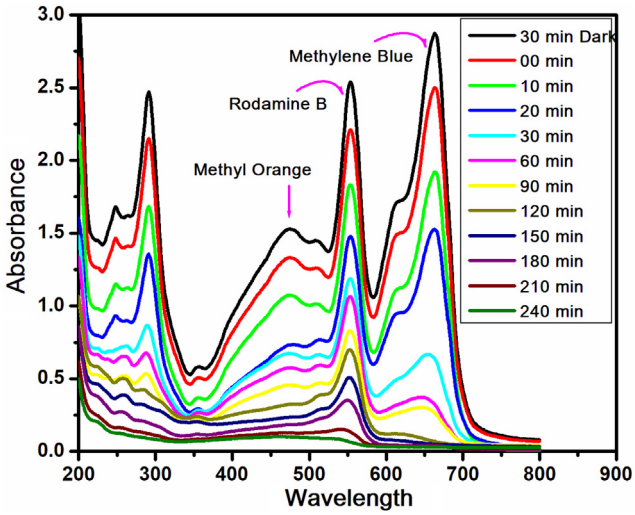


**Fig. 13.** Degradation of mixture of dyes using ZT-2:1 catalyst.

$$h^{+}_{VB} + H_2O \rightarrow H^{+} + OH^{\bullet} \quad (6)$$

$$Dye + HO^{\bullet} \rightarrow CO_2 + H_2O \text{ (non-toxic product)} \quad (7)$$

$$Dye + ZT[h^{+}_{VB}] \rightarrow \text{oxidation products} \quad (8)$$

$$Dye + ZT[e^{-}_{CB}] \rightarrow \text{reduction products} \quad (9)$$

Also, effect of loading of the catalyst has been studied by using different amount of catalyst for degradation reaction. On increasing the catalyst loading, more number of catalytic sites are available for the reaction and accelerate the degradation reaction. Fig. 12, shows progress of the reactions studied by using 0.25 gm/L, 0.50 gm/L and 1gm/L catalyst loading.

### 3.3. Photocatalytic degradation of mixture of dyes:

As we know that, industrial effluent from textile industries may have mixture of dyes. Here we have studied the photocatalytic degradation of mixture of three dyes namely, methyl orange, methylene blue and rhodamine B by using ZnTi-2:1 catalyst. The progress of the reaction has been monitored by UV–Visible analysis (Fig. 13). The degradation of the three dyes has been efficiently carried out by using this catalyst.

### 3.4. Photocatalytic degradation of tetracycline antibiotic:

Fig. 14 shows UV–visible absorption spectra of tetracycline antibiotic in the suspension of ZnTi-2:1 (100 mg) at different irradiation time. From figure, the maximum absorption peaks ($\lambda_{max}$) of tetracycline antibiotic are shown at ~270 nm and ~368 nm at zero time; which have been gradually decreased during the time illumination. It reaches the highest removal efficiency within only 60 min agitation with initial 20 ppm tetracycline antibiotic concentration. Furthur, during the photodegradation reaction the red shift has been observed for UV–Visible characteristic absorption peak from ~ 368 nm to ~ 374 nm during absorption–desorption and after irradiation the peak have been completely disappears.

### 3.5. Recyclability of the catalyst:

Recyclability is the one of the important advantage of heterogeneous catalyst over the homogeneous and liquid catalysts. We have performed the recyclability study by using most active

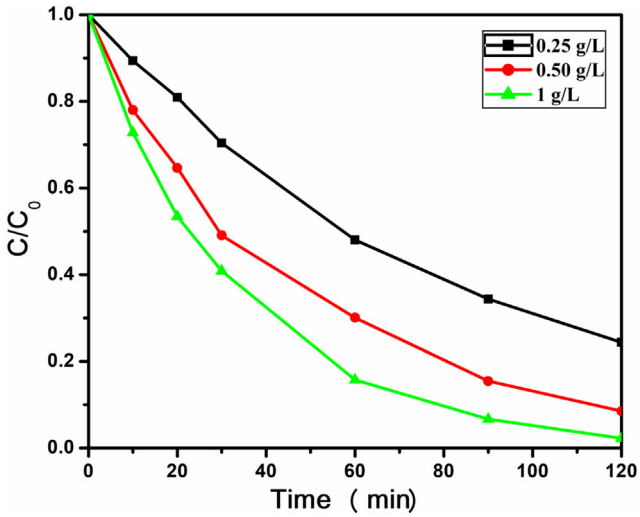


**Fig. 12.** Degradation of MB dye using different amount of ZT-2:1 as catalyst.

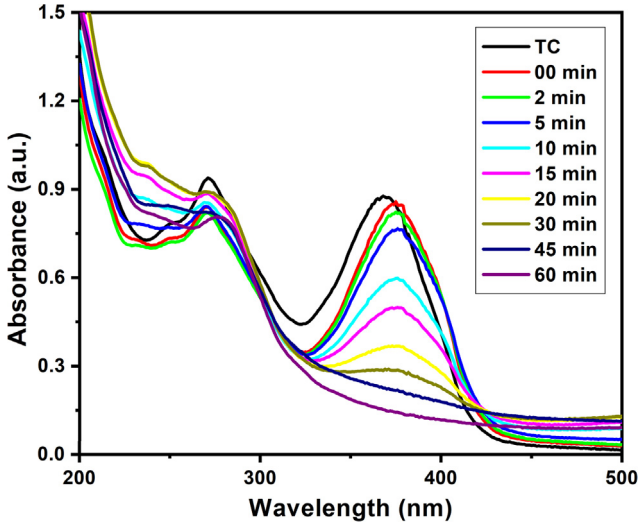


**Fig. 14.** Degradation of tetracycline using ZT-2:1 catalyst.

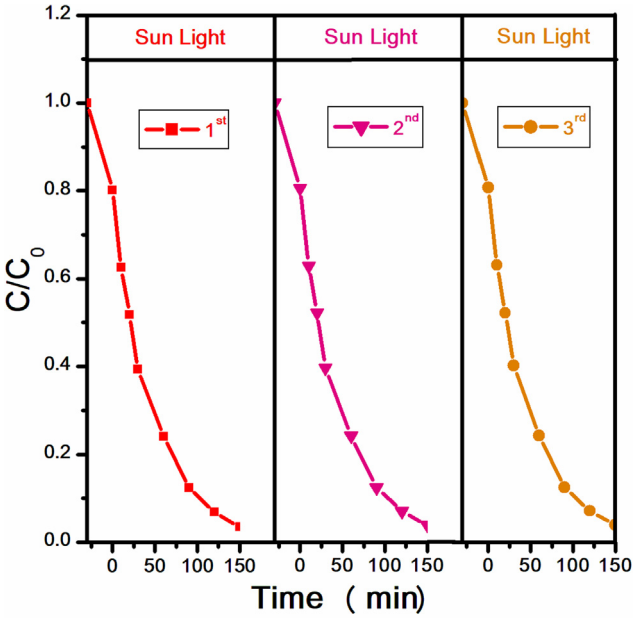


**Fig. 15.** Recyclability of ZT-2:1 for degradation of MB.

ZnTi-2:1 catalyst for degradation of methylene blue dye and the results obtained are shown in Fig. 15. During each cycle, we have separated the catalyst by centrifugation, washed with ethanol and water and dried. This recycled catalyst has been directly used for next recycle. The catalyst has been successfully reused for three cycles and in all three cycles, it has shown almost similar activity.

## 4. Conclusion

In this study, have successfully prepared ZnO/$TiO_2$ and $TiZn_2O_4$/ZnO nano-composites by using hydrothermal methods. XRD, SEM and TEM shown that the prepared catalysts are nanocrystalline in nature. Further, SEM shows the rod and spherical particles in the catalysts. These as-prepared nanocomposites has shown good efficacy for photocatalytic degradation of methylene blue dye, mixture of dyes and emerging contaminant tetracycline. ZnTi-2:1 catalyst has been recycled for three times without loss in activity.

## Declaration of Competing Interest

The authors declare that they have no known competing financial interests or personal relationships that could have appeared to influence the work reported in this paper.

## Acknowledgement

RSS deeply acknowledges to University Grants Commission (UGC), New Delhi for providing Senior Research Fellowship (Ref. No. 22/12/2013(ii) EU-V and Sr. No. 2121310321).

## References

[1] K. Sathiyan, R. Bar-Ziv, O. Mendelson, T. Zidki, Controllable synthesis of $TiO_2$ nanoparticles and their photocatalytic activity in dye degradation, Materials Research Bulletin 126 (2020) 110842.
[2] P.C.L. Muraro, S.R. Mortari, B.S. Vizzotto, G. Chuy, C. Dos Santos, L.F.W. Brum, W.L. da Silva, Iron oxide nanocatalyst with titanium and silver nanoparticles: Synthesis, characterization and photocatalytic activity on the degradation of Rhodamine B dye, Scientific reports 10 (2020) 1–9.
[3] W.R. Thalgaspitiya, T.K. Kapuge, J. He, B. Deljoo, A.G. Meguerdichian, M. Aindow, S.L. Suib, Multifunctional transition metal doped titanium dioxide reduced graphene oxide composites as highly efficient adsorbents and photocatalysts, Microporous and Mesoporous Materials 307 (2020) 110521.
[4] S. Rajagopal, B. Paramasivam, K. Muniyasamy, Photocatalytic removal of cationic and anionic dyes in the textile wastewater by H2O2 assisted $TiO_2$ and micro-cellulose composites, Separation and Purification Technology 252 (2020) 117444.
[5] D.A. Yaseen, M. Scholz, Textile dye wastewater characteristics and constituents of synthetic effluents: a critical review, International journal of environmental science and technology 16 (2) (2019) 1193–1226.
[6] J. Wang, D. Zhi, H. Zhou, X. He, D. Zhang, Evaluating tetracycline degradation pathway and intermediate toxicity during the electrochemical oxidation over a $Ti/Ti_4O_7$ anode, Water research 137 (2018) 324–334.
[7] M. Khodadadi, M. Ehrampoush, M. Ghaneian, A. Allahresani, A. Mahvi, Synthesis and characterizations of $FeNi_3$@ $SiO_2$@ $TiO_2$ nanocomposite and its application in photo-catalytic degradation of tetracycline in simulated wastewater, Journal of Molecular Liquids 255 (2018) 224–232.
[8] Q. Qi, T. Zhang, Q. Yu, R. Wang, Y. Zeng, L. Liu, H. Yang, Properties of humidity sensing ZnO nanorods-base sensor fabricated by screen-printing, Sensors and Actuators B: Chemical 133 (2008) 638–643.
[9] C. Wang, H. Liu, Y. Qu, $TiO_2$-based photocatalytic process for purification of polluted water: Bridging fundamentals to applications, Journal of Nanomaterials 2013 (2013).
[10] M.K. Patil, S. Shaikh, I. Ganesh, Recent advances on TiO2 thin Film Based Photocatalytic Applications A Review, Current Nanoscience 11 (2015) 271–285.
[11] P. Margan, M. Haghighi, Hydrothermal-assisted sol–gel synthesis of Cd-doped $TiO_2$ nanophotocatalyst for removal of acid orange from wastewater, Journal of Sol-Gel Science and Technology 81 (2017) 556–569.
[12] L. Liu, F. Chen, F. Yang, Y. Chen, J. Crittenden, Photocatalytic degradation of 2,4-dichlorophenol using nanoscale Fe/TiO2, Chemical Engineering Journal 181–182 (2012) 189–195.
[13] R.P. Barkul, M.K. Patil, S.M. Patil, V.B. Shevale, S.D. Delekar, Sunlight-assisted photocatalytic degradation of textile effluent and Rhodamine B by using iodine doped $TiO_2$ nanoparticles, Journal of Photochemistry and Photobiology A: Chemistry 349 (2017) 138–147.
[14] Y. Liu, C. Xie, J. Li, T. Zou, D. Zeng, New insights into the relationship between photocatalytic activity and photocurrent of $TiO_2/WO_3$ nanocomposite, Applied Catalysis A: General 433-434 (2012) 81–87.
[15] R.S. Sutar, R.P. Barkul, M.K. Patil, Visible Light Assisted Photocatalytic Degradation of Methylene Blue Dye and Mixture of Dyes Using $ZrO_2$-$TiO_2$ Nanocomposites, Current Nanoscience 16 (2020) 1–10.
[16] S. Chen, W. Zhao, W. Liu, S. Zhang, Preparation, characterization and activity evaluation of p–n junction photocatalyst p-ZnO/n-$TiO_2$, Applied Surface Science 255 (2008) 2478–2484.
[17] J. Deng, B. Yu, Z. Lou, L. Wang, R. Wang, T. Zhang, Facile synthesis and enhanced ethanol sensing properties of the brush-like ZnO–$TiO_2$ heterojunctions nanofibers, Sensors and Actuators B: Chemical 184 (2013) 21–26.
[18] Y. Ku, Y.-H. Huang, Y.-C. Chou, Preparation and characterization of ZnO/$TiO_2$ for the photocatalytic reduction of Cr(VI) in aqueous solution, Journal of Molecular Catalysis A: Chemical 342–343 (2011) 18–22.
[19] R. Peng, S. Banerjee, G. Sereda, R.T. Koodali, $TiO_2$–$SiO_2$ mixed oxides: Organic ligand templated controlled deposition of titania and their photocatalytic activities for hydrogen production, International Journal of Hydrogen Energy 37 (2012) 17009–17018.
[20] C. Ren, W. Qiu, Y. Chen, Physicochemical properties and photocatalytic activity of the $TiO_2/SiO_2$ prepared by precipitation method, Separation and Purification Technology 107 (2013) 264–272.
[21] B. Palanisamy, C.M. Babu, B. Sundaravel, S. Anandan, V. Murugesan, Sol–gel synthesis of mesoporous mixed $Fe_2O_3/TiO_2$ photocatalyst: Application for degradation of 4-chlorophenol, Journal of Hazardous Materials 252-253 (2013) 233–242.
[22] G. Yang, Z. Yan, T. Xiao, Preparation and characterization of $SnO_2$/ZnO/$TiO_2$ composite semiconductor with enhanced photocatalytic activity, Applied Surface Science 258 (2012) 8704–8712.
[23] B.J. Ma, J.S. Kim, C.H. Choi, S.I. Woo, Enhanced hydrogen generation from methanol aqueous solutions over Pt/$MoO_3/TiO_2$ under ultraviolet light, International Journal of Hydrogen Energy 38 (2013) 3582–3587.
[24] O. Mekasuwandumrong, P. Pawinrat, P. Praserthdam, J. Panpranot, Effects of synthesis conditions and annealing post-treatment on the photocatalytic activities of ZnO nanoparticles in the degradation of methylene blue dye, Chemical Engineering Journal 164 (2010) 77–84.
[25] K.-T. Byun, K.W. Seo, I.-W. Shim, H.-Y. Kwak, Syntheses of ZnO and ZnO-coated $TiO_2$ nanoparticles in various alcohol solutions at multibubble sonoluminescence (MBSL) condition, Chemical Engineering Journal 135 (2008) 168–173.
[26] T.G. Venkatesha, Y. Arthoba Nayaka, R. Viswanatha, C.C. Vidyasagar, B.K. Chethana, Electrochemical synthesis and photocatalytic behavior of flower shaped ZnO microstructures, Powder Technology 225 (2012) 232–238.
[27] R. Shi, P. Yang, X. Dong, Q. Ma, A. Zhang, Growth of flower-like ZnO on ZnO nanorod arrays created on zinc substrate through low-temperature hydrothermal synthesis, Applied Surface Science 264 (2013) 162–170.
[28] S. Suwanboon, P. Amornpitoksuk, A. Sukolrat, N. Muensit, Optical and photocatalytic properties of La-doped ZnO nanoparticles prepared via precipitation and mechanical milling method, Ceramics International 39 (2013) 2811–2819.

[29] H. Ma, P.L. Williams, S.A. Diamond, Ecotoxicity of manufactured ZnO nanoparticles – A review, Environmental Pollution 172 (2013) 76–85.
[30] W. Xie, Y. Li, W. Shi, L. Zhao, X. Zhao, P. Fang, F. Zheng, S. Wang, Novel effect of significant enhancement of gas-phase photocatalytic efficiency for nano ZnO, Chemical Engineering Journal 213 (2012) 218–224.
[31] J. Kim, H. Jeong, J.-Y. Park, Patterned horizontal growth of ZnO nanowires on $SiO_2$ surface, Current Applied Physics 13 (2) (2013) 425–429.
[32] S. Singh, V.C. Srivastava, S.L. Lo, T.K. Mandal, G. Naresh, Morphology-controlled green approach for synthesizing the hierarchical self-assembled 3D porous ZnO superstructure with excellent catalytic activity, Microporous and Mesoporous Materials 239 (2017) 296–309.
[33] T.K. Jana, A. Pal, K. Chatterjee, Self assembled flower like CdS–ZnO nanocomposite and its photo catalytic activity, Journal of Alloys and Compounds 583 (2014) 510–515.
[34] E.A. Araújo Júnior, F.X. Nobre, G.d.S. Sousa, L.S. Cavalcante, M. Rita de Morais Chaves Santos, F.L. Souza, J.M. Elias de Matos, Synthesis, growth mechanism, optical properties and catalytic activity of ZnO microcrystals obtained via hydrothermal processing, RSC, Advances 7 (39) (2017) 24263–24281.
[35] T.A. Thu Do, H.T. Giang, D.o. Van Huong, P.Q. Ngan, G.H. Thai, D.T. Thu, T.D. Lam, Correlation between photoluminescence spectra with gas sensing and photocatalytic activities in hierarchical ZnO nanostructures, RSC, Advances 7 (16) (2017) 9826–9832.
[36] G.S. Pozan, A. Kambur, Significant enhancement of photocatalytic activity over bifunctional ZnO–$TiO_2$ catalysts for 4-chlorophenol degradation, Chemosphere 105 (2014) 152–159.
[37] P.E. de Jongh, E.A. Meulenkamp, D. Vanmaekelbergh, J.J. Kelly, Charge Carrier Dynamics in Illuminated, Particulate ZnO Electrodes, The Journal of Physical Chemistry B 104 (2000) 7686–7693.
[38] Y. Jiang, M. Wu, X. Wu, Y. Sun, H. Yin, Low-temperature hydrothermal synthesis of flower-like ZnO microstructure and nanorod array on nanoporous $TiO_2$ film, Materials Letters 63 (2009) 275–278.
[39] Z. Liu, X. Zhang, S. Nishimoto, M. Jin, D.A. Tryk, T. Murakami, A. Fujishima, Highly Ordered $TiO_2$ Nanotube Arrays with Controllable Length for Photoelectrocatalytic Degradation of Phenol, The Journal of Physical Chemistry C 112 (2008) 253–259.
[40] N.J. Ridha, F.K.M. Alosfur, H.B.A. Kadhim, L.H. Aboud, N. Al-Dahan, Novel method to synthesis ZnO nanostructures via irradiation zinc acetate with a nanosecond laser for photocatalytic applications, Journal of Materials Science: Materials in Electronics 31 (12) (2020) 9835–9845.
[41] H. Zhang, R. Zong, Y. Zhu, Photocorrosion Inhibition and Photoactivity Enhancement for Zinc Oxide via Hybridization with Monolayer Polyaniline, The Journal of Physical Chemistry C 113 (2009) 4605–4611.
[42] L. Zheng, Y. Zheng, C. Chen, Y. Zhan, X. Lin, Q. Zheng, K. Wei, J. Zhu, Network Structured $SnO_2$/ZnO Heterojunction Nanocatalyst with High Photocatalytic Activity, Inorganic Chemistry 48 (2009) 1819–1825.
[43] H. Wang, S. Baek, J. Lee, S. Lim, High photocatalytic activity of silver-loaded ZnO-$SnO_2$ coupled catalysts, Chemical Engineering Journal 146 (2009) 355–361.
[44] Y. Izumi, T. Itoi, S. Peng, K. Oka, Y. Shibata, Site Structure and Photocatalytic Role of Sulfur or Nitrogen-Doped Titanium Oxide with Uniform Mesopores under Visible Light, The Journal of Physical Chemistry C 113 (2009) 6706–6718.
[45] P. Li, G. Zhao, X. Cui, Y. Zhang, Y. Tang, Constructing Stake Structured $TiO_2$-NTs/Sb-Doped $SnO_2$ Electrode Simultaneously with High Electrocatalytic and Photocatalytic Performance for Complete Mineralization of Refractory Aromatic Acid, The Journal of Physical Chemistry C 113 (2009) 2375–2383.
[46] F. Xiao, F. Wang, X. Fu, Y. Zheng, A green and facile self-assembly preparation of gold nanoparticles/ZnO nanocomposite for photocatalytic and photoelectrochemical applications, Journal of Materials Chemistry 22 (2012) 2868–2877.
[47] F. Xiao, Self-assembly preparation of gold nanoparticles-$TiO_2$ nanotube arrays binary hybrid nanocomposites for photocatalytic applications, Journal of Materials Chemistry 22 (2012) 7819–7830.
[48] F. Xiao, An efficient layer-by-layer self-assembly of metal-$TiO_2$ nanoring/nanotube heterostructures, M/T-NRNT (M = Au, Ag, Pt), for versatile catalytic applications, Chemical Communications 48 (2012) 6538–6540.
[49] A. Kubacka, M. Ferrer, M. Fernández-García, Kinetics of photocatalytic disinfection in $TiO_2$-containing polymer thin films: UV and visible light performances, Applied Catalysis B: Environmental 121-122 (2012) 230–238.
[50] S. Hernández, V. Cauda, D. Hidalgo, V. Farías Rivera, D. Manfredi, A. Chiodoni, F. C. Pirri, Fast and low-cost synthesis of 1D ZnO–$TiO_2$ core–shell nanoarrays: Characterization and enhanced photo-electrochemical performance for water splitting, Journal of Alloys and Compounds 615 (2014) S530–S537.
[51] E. Colombo, W. Li, S.K. Bhangu, M. Ashokkumar, Chitosan microspheres as a template for $TiO_2$ and ZnO microparticles: studies on mechanism, functionalization and applications in photocatalysis and $H_2S$ removal, RSC Advances 7 (2017) 19373–19383.
[52] A.A. Kostedt, D.W. Ismail, Mazyck, Impact of Heat Treatment and Composition of ZnO−$TiO_2$ Nanoparticles for Photocatalytic Oxidation of an Azo Dye, Industrial & Engineering Chemistry Research 47 (2008) 1483–1487.
[53] D.L. Liao, C.A. Badour, B.Q. Liao, Preparation of nanosized $TiO_2$/ZnO composite catalyst and its photocatalytic activity for degradation of methyl orange, Journal of Photochemistry and Photobiology A: Chemistry 194 (2008) 11–19.
[54] H. Yu, Z. Zhang, M. Han, X. Hao, F. Zhu, A General Low-Temperature Route for Large-Scale Fabrication of Highly Oriented ZnO Nanorod/Nanotube Arrays, Journal of the American Chemical Society 127 (2005) 2378–2379.
[55] Q. Yu, W. Fu, C. Yu, H. Yang, R. Wei, M. Li, S. Liu, Y. Sui, Z. Liu, M. Yuan, G. Zou, G. Wang, C. Shao, Y. Liu, Fabrication and Optical Properties of Large-Scale ZnO Nanotube Bundles via a Simple Solution Route, The Journal of Physical Chemistry C 111 (2007) 17521–17526.
[56] Y. Lei, G. Zhao, M. Liu, Z. Zhang, X. Tong, T. Cao, Fabrication, Characterization, and Photoelectrocatalytic Application of ZnO Nanorods Grafted on Vertically Aligned $TiO_2$ Nanotubes, The Journal of Physical Chemistry C 113 (2009) 19067–19076.
[57] M. Zhang, T. An, X. Liu, X. Hu, G. Sheng, J. Fu, Preparation of a high-activity ZnO/$TiO_2$ photocatalyst via homogeneous hydrolysis method with low temperature crystallization, Materials Letters 64 (2010) 1883–1886.
[58] Q.-Y. Li, H.-W. Sun, Q. Wei, S.-B. Sun, J.-G. Liu, S.-P. Cui, Z.-R. Nie, Synthesis and high photocatalytic performance of a novel hollow meso-$TiO_2$/ZnO composite microsphere, Journal of Sol-Gel Science and Technology 95 (2020) 344–352.
[59] Z. Liu, F. Jiang, R. Liu, Study on preparation of ZnO-$TiO_2$ composite photocatalyst and its properties, in, Applied Mechanics and Materials (2012) 1008–1011.
[60] Z.H. Li, Y.L. Bai, Preparation of $TiO_2$/ZnO composite nanoparticles and their UV-shielding properties, Journal of Tianjin Polytechnic University 36 (2017) 49–53.
[61] H.M. Umair Arshad, H. Anwar, Y. Javed, M.Y. Naz, A. Ghaffar, M.Z. Khan, Z. Farooq, Investigation of photo-catalytic degradation of methylene orange dye using titanium dioxide–zinc oxide nanocomposites, Materials Research Express 6 (2019) 125009.
[62] M.A. Habib, M.T. Shahadat, N.M. Bahadur, I.M.I. Ismail, A.J. Mahmood, Synthesis and characterization of ZnO-$TiO_2$ nanocomposites and their application as photocatalysts, International Nano Letters 3 (2013) 5.
[63] H. Xu, W. Liu, L. Cao, G. Su, R. Duan, Preparation of porous $TiO_2$/ZnO composite film and its photocathodic protection properties for 304 stainless steel, Applied Surface Science 301 (2014) 508–514.
[64] S. Moradi, P. Aberoomand-Azar, S. Raeis-Farshid, S. Abedini-Khorrami, M.H. Givianrad, The effect of different molar ratios of ZnO on characterization and photocatalytic activity of $TiO_2$/ZnO nanocomposite, Journal of Saudi Chemical Society 20 (2016) 373–378.
[65] M. Chegeni, S.K. Pour, B. Faraji Dizaji, Synthesis and characterization of novel antibacterial Sol-gel derived $TiO_2$/$Zn_2TiO_4$/Ag nanocomposite as an active agent in Sunscreens, Ceramics International 45 (2019) 24413–24418.
[66] R.B. Pinto, P. Peralta-Zamora, F. Wypych, Fabrication of ZnO-$Zn_2TiO_4$ nanocomposite from zinc hydroxide nitrate and its photocatalytic efficiency, Journal of Photochemistry and Photobiology A: Chemistry 353 (2018) 46–52.
[67] K. Takase, H. Nishizawa, A. Onda, K. Yanagisawa, S. Yin, Synthesis and characterization of glycolate precursors to $MTiO_3$, M = Ni2+, Co2+, Zn2+, Journal of Asian Ceramic Societies 5 (2017) 482–488.
[68] J.S.J. Hargreaves, Some considerations related to the use of the Scherrer equation in powder X-ray diffraction as applied to heterogeneous catalysts, Catalysis, Structure and Reactivity 2 (1-4) (2016) 33–37.
[69] J. Arin, S. Thongtem, A. Phuruangrat, T. Thongtem, Characterization of ZnO–$TiO_2$ and zinc titanate nanoparticles synthesized by hydrothermal process, Research on Chemical Intermediates 43 (5) (2017) 3183–3195.
[70] X.-Y. Chen, X.-Z. Wang, F.-J. Liu, G.-S. Zhang, X.-J. Song, J. Tian, H.-Z. Cui, Fabrication of porous $Zn_2TiO_4$–ZnO microtubes and analysis of their acetone gas sensing properties, Rare Metals 40 (6) (2021) 1528–1535.